Wireless monitoring of typhoon-induced variation of dynamic characteristics of a cable-stayed bridge

Jae-Hyung Park[a], Thanh-Canh Huynh[b] and Jeong-Tae Kim[*]

*Department of Ocean Engineering, Pukyong National University, 45 Yongso-ro, Nam-gu,
Busan 608-737, Republic of Korea*

Abstract.   In this paper, wireless monitoring of typhoon-induced variation of dynamic characteristics of a cable-stayed bridge is presented. Firstly, cable-stayed bridge with the wireless monitoring system is described. Wireless vibration sensor nodes are utilized to measure accelerations from bridge deck and stay cables. Also, modal analysis methods are selected to extract dynamic characteristics. Secondly, dynamic responses of the cable-stayed bridge under the attack of two typhoons are analyzed by estimating relationships between wind velocity and dynamic characteristics. Wind-induced variations of deck and cable vibration responses are examined based on the field measurements under the two consecutive typhoons, Bolaven and Tembin. Finally, time-varying analyses are performed to investigate non-stationary random properties of the dynamic responses under the typhoons.

Keywords: wireless monitoring; typhoon-induced variation; dynamic characteristics; cable-stayed bridge

1. Introduction

Cable-stayed bridges are sensitive to wind because of the relative lightness, flexibility and low damping; therefore, the aerodynamic performance of the bridges is one of important concerns in their design processes (Zhou *et al.* 2008). In the design process, however, the performance is evaluated from numerical simulations and lab-scaled experiments with various assumptions. In order to verify the design assumptions and to monitor the structural performance of the bridges, many structural health monitoring (SHM) systems have been installed in the bridges (Atkan *et al.* 2003, Ko and Ni 2005, Yi *et al.* 2013, Li *et al.* 2014, Huang and Nagarajaiah 2014).

The installation of the conventional wired SHM systems requires very high costs. The cost can be greatly reduced through the adoption of wireless sensor. Many advantages of wireless sensor systems have been discussed by Spencer *et al.* (2004), Lynch and Loh (2006), Nagayama *et al.* (2007), Jang *et al.* (2010) and Kim *et al.* (2011). One of the advantages is the autonomous operation enabled by on-board computation units which allows the long-term health monitoring without off-line interference of experts (Cho *et al.* 2010).

[*]Corresponding author, Professor, E-mail: idis@pknu.ac.kr
[a] BK21Plus Professor, E-mail: cross96@gmail.com
[b] Ph.D. Student, E-mail: ce.huynh@gmail.com

A research team at Pukyong National University, Korea, has developed vibration sensor systems (Ho *et al.* 2012b, Nguyen *et al.* 2013, Ho *et al.* 2014). During the field experiments on a real cable-stayed bridge (Hwamyung Bridge, Busan, Korea), the long-term performance of the wireless sensor system has been evaluated with regarding to the measurement of vibration responses, the communication between wireless sensors, the solar-powered battery supply dependent on weather conditions, and the survivability of sensors with respect to usage period (Ho *et al.* 2012a). Just after the construction, the bridge experienced two consecutive typhoons, Bolaven and Tembin, in year 2012 (Evans and Falvey 2012). During the events, the wireless sensor system recorded data of wind speeds and vibration responses from a few survived sensor nodes. Kim *et al.* (2014) have examined the performance of the wireless monitoring of stay cables under the typhoons and also the effect of the typhoons on the variation of cable forces.

Many researchers have investigated the wind effect on dynamic characteristics such as natural frequency and damping. The dynamic responses of the cable-stayed bridges are consistently associated with the aerodynamics such as turbulence, vortex, buffeting, galloping and so on (Bietry *et al.* 1995, Mishra *et al.* 2007, Zhou *et al.* 2008, Larsen and Larose 2015). Most researches have focused on analyzing wind-induced variation of dynamic characteristics of the cable-stayed bridges for the various wind conditions. As a remaining issue, the dynamic responses of the bridges become non-stationary since the wind velocity varies rapidly under the typhoon. Therefore, the non-stationary random vibration responses should be examined by time-varying analysis such as the short-time Fourier transform (STFT) or wavelet transformation.

In this paper, wireless monitoring of typhoon-induced variation of dynamic characteristics of a cable-stayed bridge is presented. Firstly, cable-stayed bridge with the wireless monitoring system is described. Wireless vibration sensor nodes developed by Kim *et al.* (2013) are utilized to measure accelerations from bridge deck and stay cables. Also, modal analysis methods are selected to extract dynamic characteristics. Secondly, dynamic responses of the cable-stayed bridge under the attack of the two typhoons are analyzed by estimating relationships between wind velocity and dynamic characteristics. Wind-induced changes in deck and cable vibration responses are examined based on the field measurements under the two consecutive typhoons, Bolaven and Tembin. Finally, time-varying analyses are performed to investigate non-stationary random properties of the dynamic responses under the typhoons.

2 Cable-stayed bridge with wireless monitoring system

2.1 Description of Hwamyung cable-stayed bridge

As shown in Fig. 1, the Hwamyung cable-stayed bridge, Busan, Korea, was selected for wirelessly monitoring typhoon-induced dynamic responses. The bridge was constructed by Hyundai Engineering & Construction Co., Ltd., from December 2004 to July 2012. As schematized in Fig. 2, the bridge consists of three spans including a 270-m central main span between two pylons and two 115-m side spans connecting east and west approaches. The height of two pylons is 65-m from deck level. The clearance of the deck is 14.7 m from the water level. The box girder is 27.8-m width and 4-m height. The bridge has total 72 cables, positioning 36 cables at each pylon. Details on the bridge are described in Ho *et al.* (2012a).

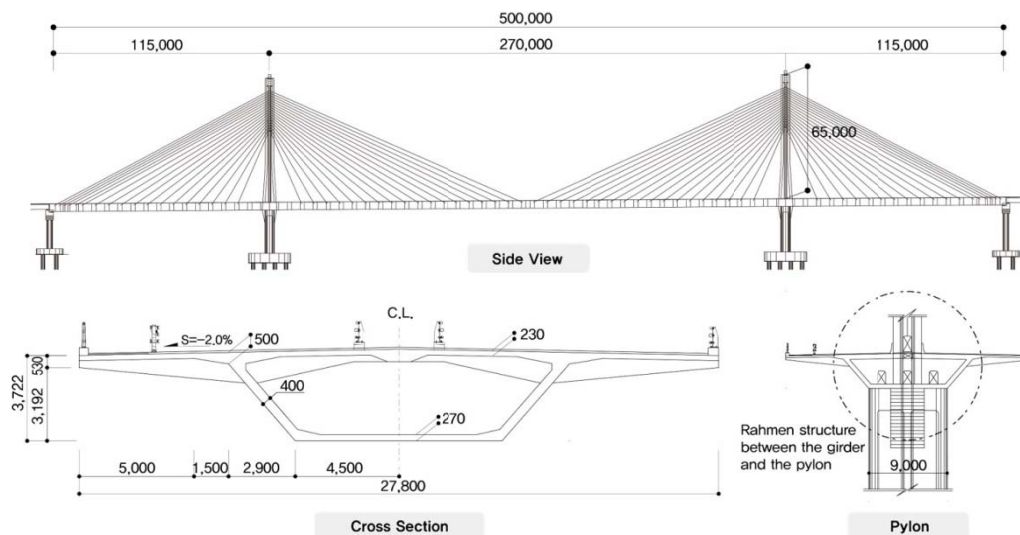Fig. 1 Hwamyung cable-stayed bridge

Fig. 2 Geometry of Hwamyung cable-stayed bridge (unit: mm)

2.2 Design of wireless monitoring system

2.2.1 Vibration sensor node

Based on the design of Imote2-platformed vibration measurement system (Nagayama and Spencer 2007, Rice and Spencer 2009, Ho *et al.* 2012b), a wireless vibration sensor node was designed as shown in Fig. 3. The high-performance sensor platform, Imote2, provided by Memsic Co. (2010), was selected to control the operation of the sensor node. For vibration monitoring, SHM-A and SHM-H sensor boards were selected. The SHM-A and SHM-H sensor boards were developed for acceleration measurement by University of Illinois at Urbana-Champaign (Rice and Spencer 2009, Jo *et al.* 2010). As shown in Fig. 3(a), the solar-powered energy harvesting is implemented by employing solar panel and rechargeable battery. Fig. 3(b) shows a prototype of the wireless sensor node which consists of four layers as 1) X-bow battery board, 2) Imote2 sensor platform, and 3) SHM-H board or SHM-A board.

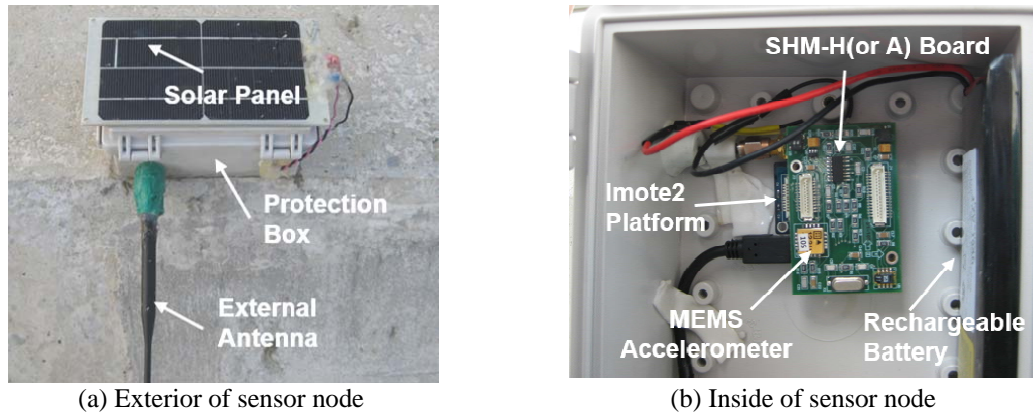(a) Exterior of sensor node   (b) Inside of sensor node

Fig. 3 Configuration of wireless sensor node

The Imote2 platform is built with 13-416 MHz PXA271 XScale processor (Memsic Co. 2010). This processor integrates with 256 kB SRAM, 32 MB flash memory and 32 MB SDRAM. It also integrates with many I/O options such as 3×UART, I2C, 2×SPI, SDIO, I2S, AC97, USB host, Camera I/F, GPIO. Therefore, Imote2 platform is very flexible in supporting different sensor types, ADC chips and radio options. A 2.4G Hz surface mount antenna which has a communication range of about 300m is equipped for each Imote2 platform.

For deck's acceleration measurement, the SHM-H sensor board is adopted to employ a SD1221 accelerometer for high-sensitivity channel, the input range $\pm$ 2 g, the sensitivity 2 V/g and the output noise 5 μg/√Hz. For cable's acceleration measurement, the SHM-A sensor board is adopted to employ the tri-axial LIS344ALH accelerometer of which its sensitivity is relatively lower and output noise is relatively higher than the SHM-H. Its core component is the 16 bit ADC with digital filter, QF4A512 ADC, for signal conditioning with customizable sampling rates. It is interfaced with the Imote2 sensor platform via SPI protocol that transmits the measured signal to the main CPU.

2.2.2 Vibration monitoring software

The embedded software for vibration monitoring is programmed for the sensor node according to the UIUC ISHMP Services Toolsuite (Illinois Structural Health Monitoring Project 2010) and PKNU SSeL-SHM Tools (Kim *et al.* 2011). As schematized in Fig. 4, the schematic of the wireless monitoring software was designed for acceleration measurement. First, the RemoteSensing component of the ISHMP Services Toolsuite is implemented for sensing. For long-term operation, the sensor nodes are embedded with the ChargerControl component to harvest environmental energies such as wind energy or solar energy. The AutoMonitor component is embedded to the gateway node to periodically wake up the sensor system and let the sensor nodes measure structural responses (Rice and Spencer 2009, Miller *et al.* 2010).

Once vibration signals are recorded, modal parameters are estimated by the PeakPicking and SSI components of the SSeL-SHM Tools. The procedure is performed in the following three major tasks: (1) power spectral density (PSD) calculation, (2) natural frequency calculation, and (3) modal parameter extraction.
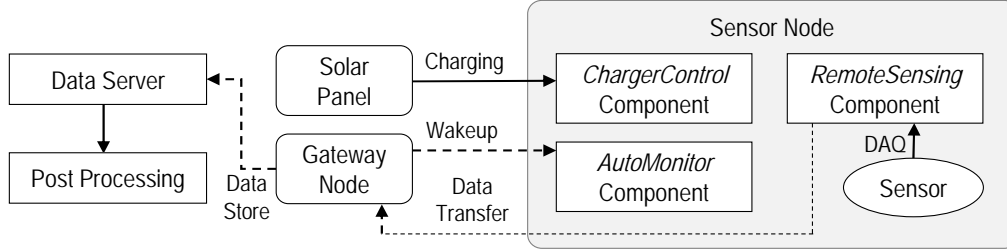
Fig. 4 Schematic of wireless monitoring for acceleration measurement

Firstly, the recorded signal is transformed into the PSD according to Welch's procedure using overlapping as follows (Bendat and Piersol 1993)

$$S_{xx}(f) = \frac{1}{n_d T} \sum_{i=1}^{n_d} |X_i(f,T)|^2$$

(1)

where X_i is the dynamic response transformed into the frequency domain (FFT transform); n_d is the number of divided segments in the time history response; and T is the data length of a divided segment.

Secondly, natural frequencies are obtained from the automated peak-picking algorithm. The basic concept of the algorithm is to search the local maxima of the PSD curve, which represent natural frequencies. The entire frequency range is divided into N number of user-selected sub-frequency ranges. By examining each sub-frequency range, the natural frequency is picked if its magnitude is the largest in the range.

Thirdly, modal parameters (i.e., natural frequency, damping ratio and mode-shape) are extracted by a stochastic subspace identification (SSI) method. The SSI method utilizes the singular value decomposition (SVD) of a block Hankel matrix with cross correlation matrix of responses as follows (Overschee and De Moor 1996)

$$\mathbf{H} \approx \begin{bmatrix} \mathbf{U_1} & \mathbf{U_2} \end{bmatrix} \begin{bmatrix} \mathbf{\Sigma_1} & 0 \\ 0 & 0 \end{bmatrix} \begin{bmatrix} \mathbf{V_1^T} \\ \mathbf{V_2^T} \end{bmatrix} = \mathbf{U_1 \Sigma_1 V_1^T}$$

(2)

where $\mathbf{H}$ is the Hankel matrix; $\mathbf{U}$, $\mathbf{V}$ are the unitary matrices; and $\mathbf{\Sigma_1}$ is the singular value matrix. The modal parameters can be identified from a system matrix which is determined from the SVD algorithm. A stabilization chart is used to find a suitable system order with the criteria which classify a mode as stable mode, unstable mode, and noise mode (Yi and Yun 2004). Once the stable modes are detected, damping ratio (ξ_i) of the ith mode is identified from the eigenvalue (λ_i) as follows:

$$\xi_i = -\operatorname{Re}(\lambda_i) / |\lambda_i|$$

(3)

Finally, the all data including raw data, PSD matrix, natural frequencies by peak-peaking and modal parameters by the SSI method is transferred to a data server. The raw data is used for post-processing.
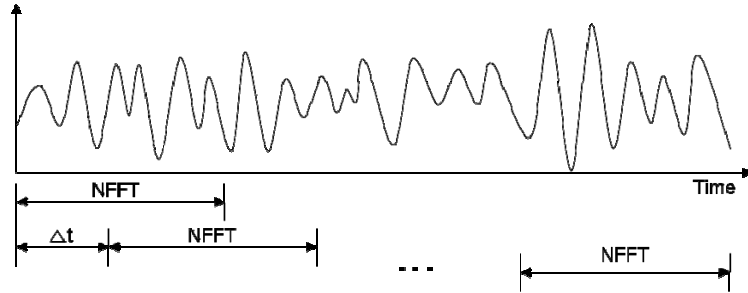
Fig. 5 Short-time Fourier transform with overlapping

2.2.3 Short-time Fourier transform analysis

In order to analyze non-stationary random signals, short-time Fourier transform (STFT) and wavelet transform are generally used. In this study, the STFT is selected for the time-varying analysis due to its simplicity by using FFT. For given time-series $x[n]$, the STFT at time n is given as (Quatieri 2001)

$$X(n, \omega) = \sum_{m=-\infty}^{\infty} x[m]w[n-m]e^{-j\omega m} \tag{4}$$

where ω is frequency and $w[n]$ is the window function which is assumed to be non-zero only in the interval $[0, N_w - 1]$.

The size of window function $w[n]$ is carefully selected by considering the time and frequency resolutions of STFT. If the long window size is selected to make fine resolution, the time resolution becomes poor, and vice versa. To overcome the disadvantage for the time-frequency resolution, an overlap method is used in this study. In Fig. 5, NFFT is the length of time window for FFT and Δt is the time resolution calculated by difference of NFFT and overlapping point

2.3 Sensor lay-out for Hwamyung cable-stayed bridge

For vibration monitoring of the Hwamyung cable-stayed bridge, twelve (12) sensor nodes (Imote2/SHM-H) including 11 leaf sensor nodes and 1 gateway node were installed on the bridge, as shown in Fig. 6. Among the leaf nodes, 6 Imote2/SHM-H sensors were placed at five locations of the deck and at the top of the west pylon (i.e., D1~D5, and P1). Five Imote2/SHM-A sensors were placed on five selected cables (i.e., C1~C5). The base station including a gateway node and a PC was installed at the nearest pylon P1 as shown in Fig. 6.

As shown in Fig. 7, the sensor nodes and the gateway node were placed in plastic boxes which have waterproof rubber gaskets for preventing the nodes from sun-heating, being absorbed and other environmental effects (e.g., rain, wind and dust). The sensor nodes were powered by Li-ion polymer rechargeable batteries (Powerizer 3.7V, 10000mAh). Solar panels (SPE-350-6) were mounted on the sensor boxes to harvest the solar energy and recharge the batteries (Nguyen *et al.* 2013).
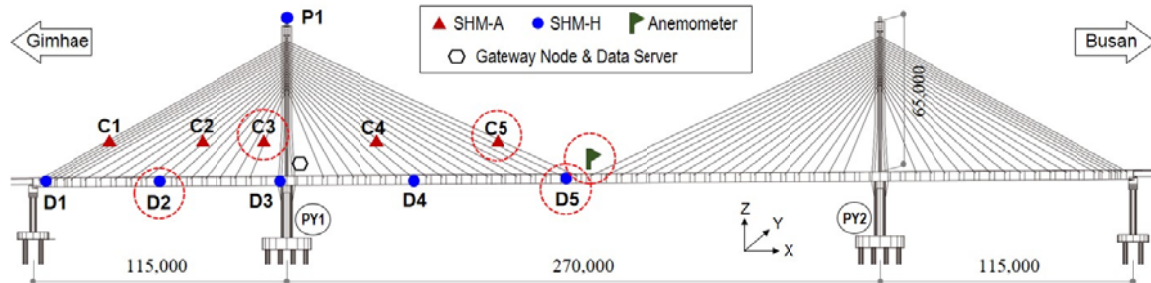
Fig. 6 Sensor layout on Hwamyung cable-stayed bridge

(a) Leaf node on Deck   (b) Leaf node on stay cable   (c) Gateway node on P1
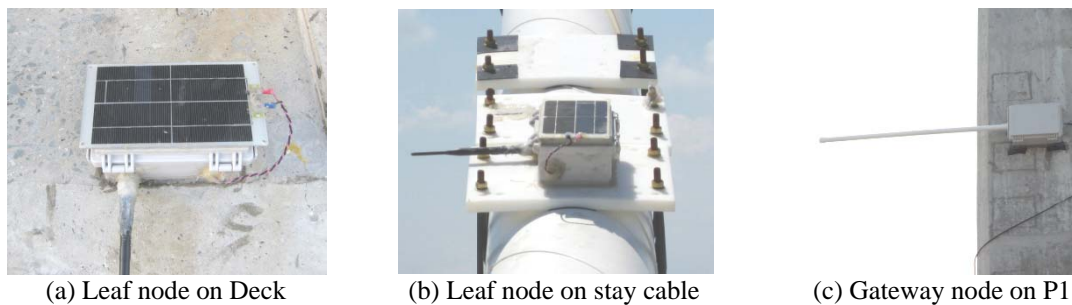
Fig. 7 Typical experimental setup for sensor nodes

As a part of the smart monitoring system, the on-site wind velocity and wind direction were monitored by using an ultrasonic wind sensor, Model 85000/RM Young, located at the middle of the bridge (HM Bridge System 2012). This device employs a 2-axis, no-moving-parts wind sensor. The wind speed range up to 70 m/s (0.1 m/s resolution) and the wind direction up to 360° (1° resolution) are suitable for field applications requiring accurate, reliable wind measurement (RM Young Co. 2014) (Kim *et al.* 2014).

Among the 11 sensor nodes except the gateway node, unfortunately, only a few sensor nodes including two deck nodes (D2 and D5) and two cable nodes (C3 and C5) had made successful monitoring and communication performances during the attacks of the two typhoon (Tembin and Bolaven). In Fig. 6, four circles with dot-line indicate the survived nodes. The deck nodes D2 and D5 are located at the center of side-span and mid-span, respectively. Also, the cable nodes C2 and C5 are located at the shortest and the longest stay-cables. Therefore, data from those nodes can give the significant information for wind-induced dynamic responses of the bridge, even though all sensor nodes were not available.

3. Vibration monitoring in cable-stayed bridge under two typhoons

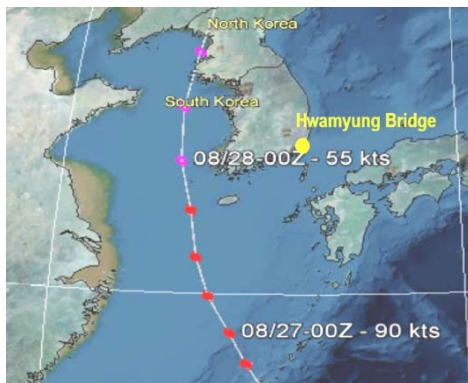### 3.1 Two consecutive typhoons

Typhoons Bolaven and Tembin passed through the Korean peninsula back-to-back on August

28 and 30, 2012, and affected the site of Hwamyung cable-stayed bridge. As shown in Fig. 8, typhoon Bolaven struck the Korean peninsula with the record of wind gusts measured up to 30 m/s (Evans and Falvey 2012). Another typhoon Tembin slammed into South Korea dumping heavy rains on southern and western regions just two days after typhoon Bolaven. As shown in Fig. 9, the maximum wind speeds recorded on-site by the ultrasonic wind meter located in the middle of the bridge (see Fig. 6) were about 20 m/s during typhoons Bolaven and Tembin. It was a quite rare event to have two typhoons passing the bridge site back to back in a few days. Therefore, there were interests on analyzing the wind-induced dynamic characteristics of the bridge under the consecutive typhoons.

3.2 Typhoon-induced variation of dynamic characteristics of the deck

3.2.1 Acceleration and frequency responses of the deck

During the two consecutive typhoons, vibration responses of the deck were wirelessly monitored by the high-sensitivity acceleration sensor nodes (Imote2/SHM-H) installed at the deck D2 and D5. As shown in Fig. 10, the deck D2 at the middle of the side-span had the maximum acceleration response about 0.008 g when the wind speed was about 20 m/s during the typhoon Bolaven. The deck D5 at the middle of mid-span had the maximum acceleration response about 0.013 g when the wind speed was about 20 m/s during the typhoon Bolaven.
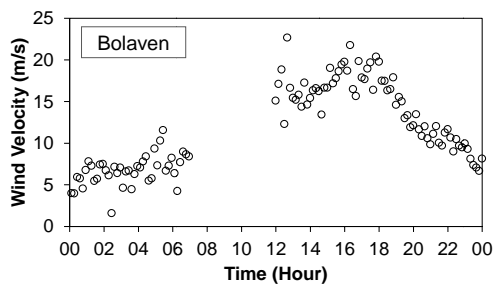

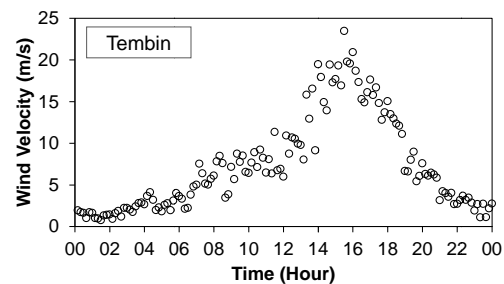(a) Tyhpoon Bolaven's path (Aug 28, 2012)   (b) Typhoon Tembin's path (Aug 30, 2012)

Fig. 8 Two consecutive typhoons: Bolaven and Tembin (Evans and Falvey 2012)

(a) Typhoon Bolaven   (b) Typhoon Tembin

Fig. 9 Measured wind velocities during two back-to-back typhoons

As shown in Fig. 11, acceleration and frequency responses of the deck were recorded for five different wind speeds: 3.72 m/s, 5.05 m/s, 11.70 m/s, 17.92 m/s, and 19.36 m/s. Fig. 11(a) shows wind-induced changes in acceleration and PSD responses measured at the deck D2. Acceleration levels change about 17 times (e.g., 0.0002g - 0.0034g) due to the change in wind speeds. The PSD responses of the deck D2 indicate the first six resonance peaks and their changes due to the change in wind speeds. Fig. 11(b) shows wind-induced changes in acceleration and PSD responses measured at the deck D5 for the five wind speeds. Acceleration levels change about 17 times (e.g., 0.0035g – 0.0052g) as the wind speeds vary 3.5~20 m/s. The PSD responses of the deck D5 indicate the first six resonance peaks and their changes due to the change in wind speeds.

Modal parameters (i.e., natural frequency, damping ratio and mode-shape) were extracted by a stochastic subspace identification (SSI) method described in Eq. (2). Fig. 12 shows the SSI's stability chart to identify natural frequencies of four modes: 1st frequency 0.419 Hz, 2nd frequency 0.692 Hz, 4th frequency 1.048 Hz, and 6th frequency 1.401 Hz (note that the mode order and noise modes follow the modes presented in Ho *et al.* (2012a)). Fig. 13 shows identified mode shapes of the four modes of the deck measured at wind speed 3.72 m/s. With the reference of the published mode shapes by Ho *et al.* (2012a), modal amplitudes of the four modes were extracted from only the deck D2 and D5 because other sensors located at deck D1, D3 and D4 powered off during the typhoon events. Note that Ho *et al.* (2012a) extracted modal parameters from all five locations (e.g., D1 ~ D5). In order to compare with the modal amplitudes extracted by Ho *et al.* (2012a), they were normalized by norm of the amplitudes at deck D3 and D5. Considered difference of measurement conditions such as wind speed and temperature, the measured modal amplitudes show consistent results as compared to the mode shapes by Ho *et al.* (2012a) as shown in Fig. 13.
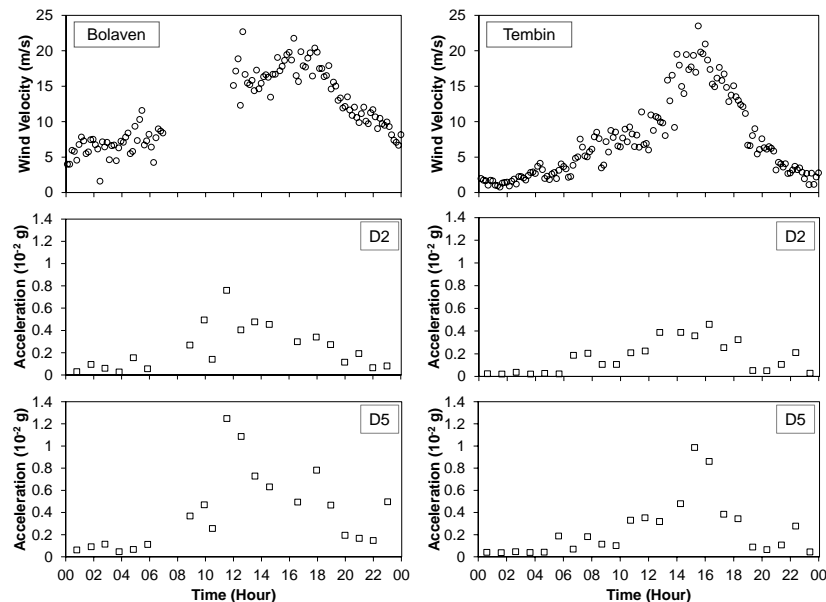

Fig. 10 Wind speeds and maximum acceleration responses at the deck D2 and D5 during two typhoons Bolaven and Tembin

(a) Acceleration and PSD responses at D2
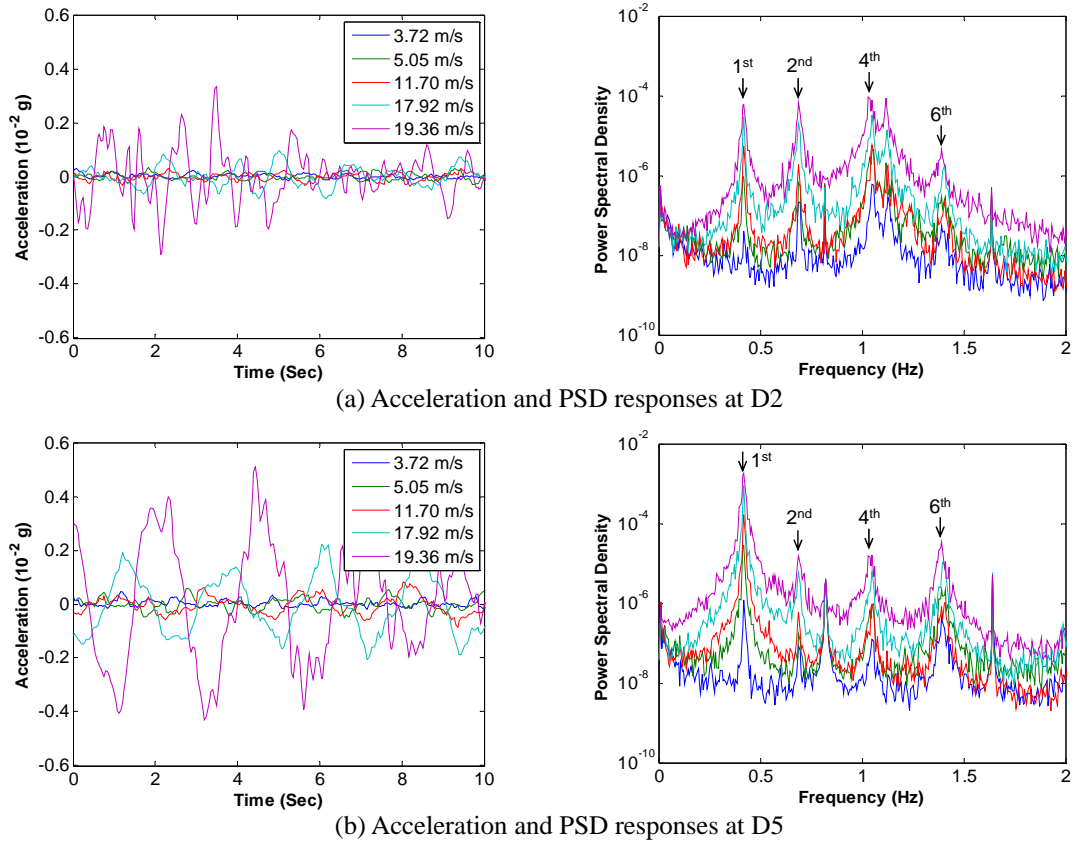

(b) Acceleration and PSD responses at D5

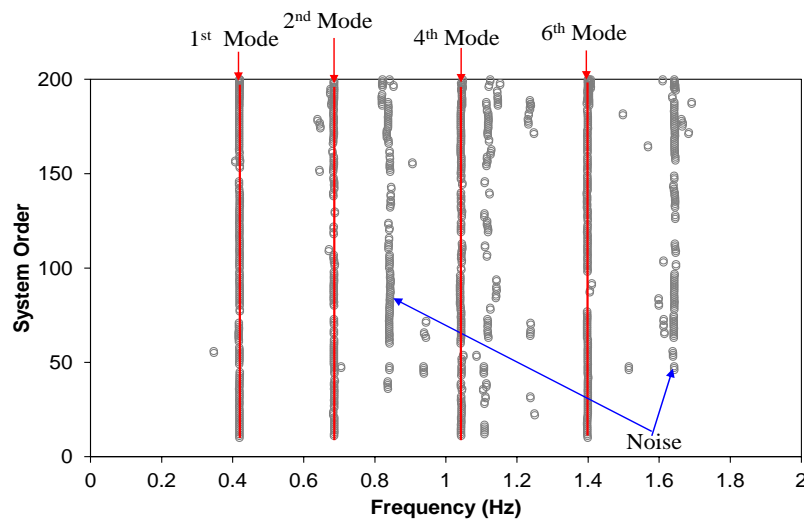Fig. 11 Acceleration and frequency responses of the deck during typhoons

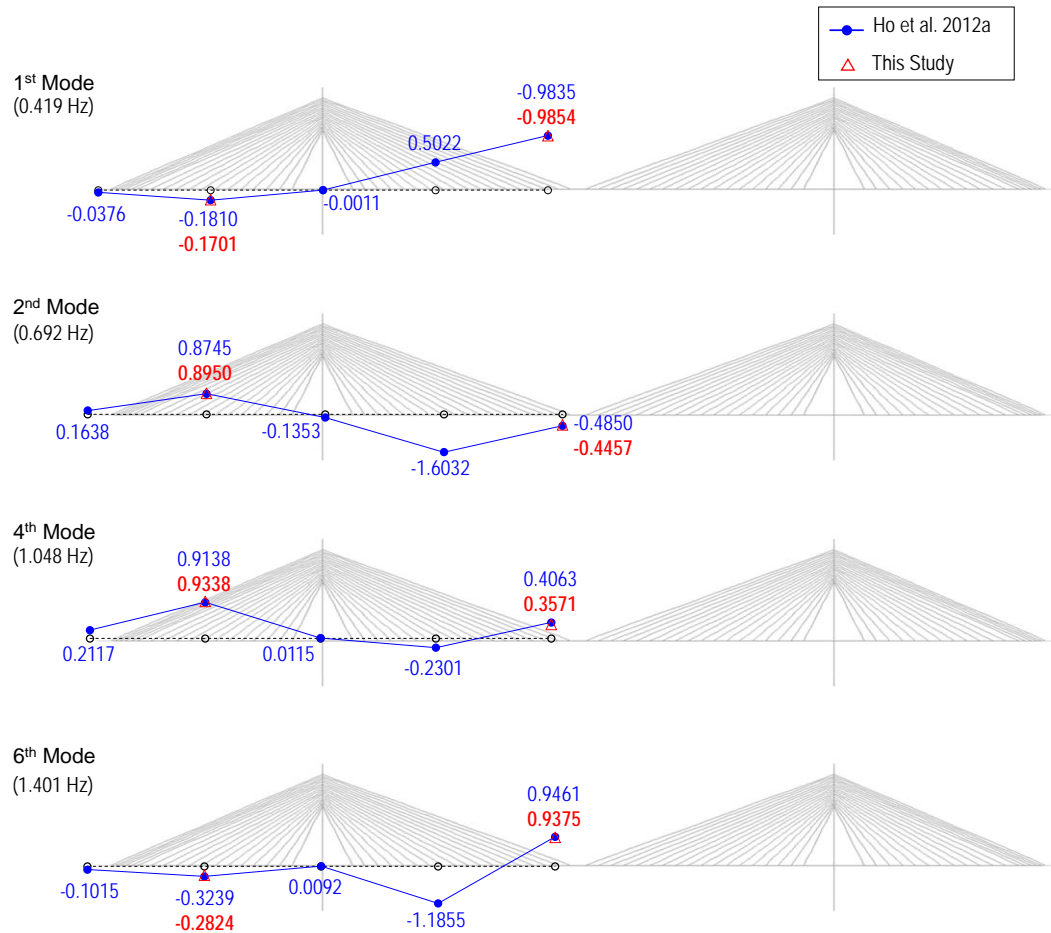Fig. 12 Modal identification of the deck by SSI's stability chart

Fig. 13 Identified mode shapes of the deck at wind speed 3.72 m/s

3.2.2 Wind velocity versus modal parameters of the deck

Firstly, the relationship between wind speeds and natural frequencies of the deck were analyzed for the four bending modes to investigate the typhoon-induced changes in dynamic characteristics of the bridge, as shown in Fig. 14. The first mode's natural frequency shows rather linear function with respect to the variation of wind speeds. For the second, fourth and sixth frequencies, the linear and quadratic functions are well-matched each other. Note that solid lines and equations in the figures are for the linear functions and dot lines represents the quadratic functions, and R_l and R_q are correlation coefficients for the linear and quadratic functions, respectively. Nonetheless of the slopes of those functions, it is clear that all four natural frequencies of the deck decrease as the increment of wind speeds. As evident by the slopes of the linear trends in Fig. 14, the changes of the first and the second frequencies (the lower-order modes) are more apparent than the fourth and the sixth frequencies (higher-order modes). Natural frequencies decrease up to about 0.6% as the wind speeds increase up to 20 m/s.
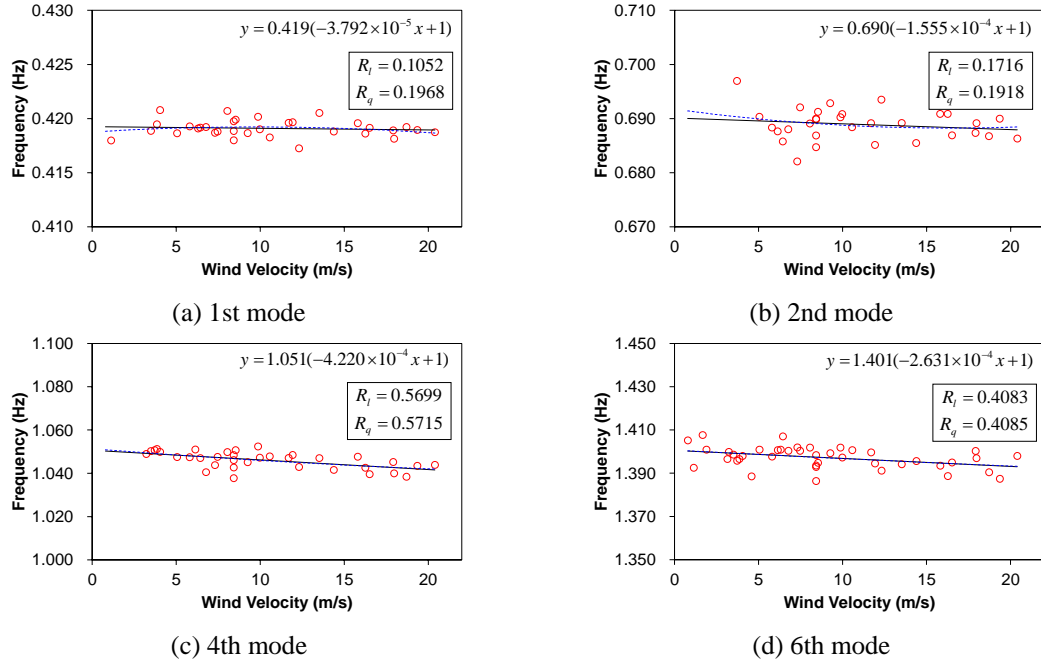
(a) 1st mode

(b) 2nd mode

(c) 4th mode

(d) 6th mode

Fig. 14 Relationships between wind velocity and four natural frequencies of the deck during typhoons

(a) 1st mode

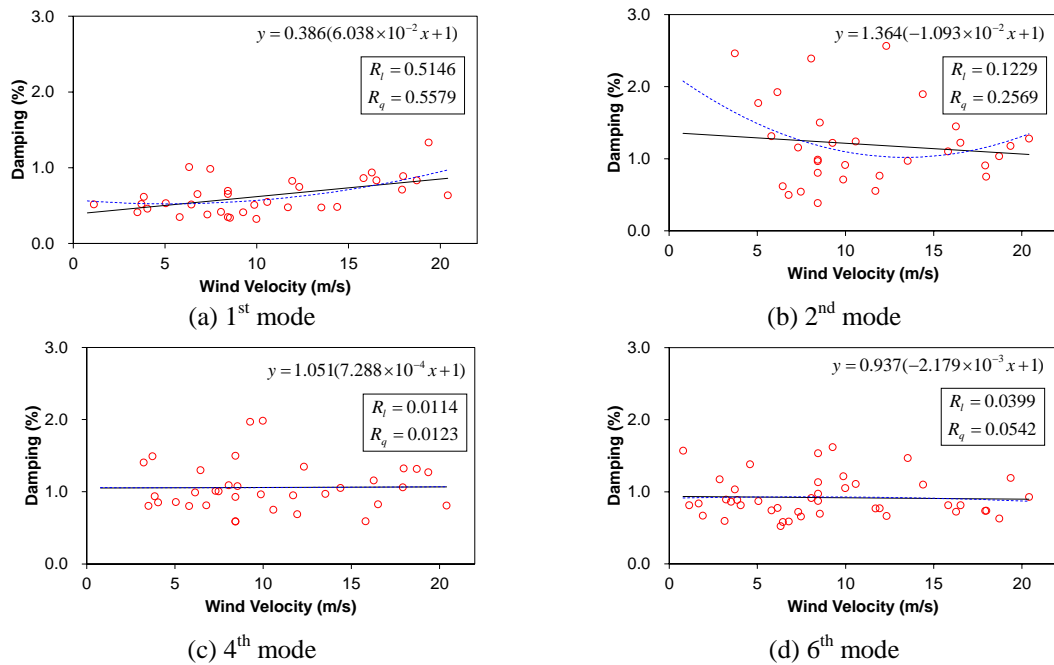(b) 2nd mode

(c) 4th mode

(d) 6th mode

Fig. 15 Relationships between wind velocity and four modal damping coefficients of the deck during typhoons

Secondly, the relationship between wind speeds and modal damping coefficients of the deck were analyzed for the four bending modes to examine the typhoon-induced changes in dynamic characteristics of the bridge. As shown in Fig. 15, the first and the second mode's damping coefficients show rather quadratic functions with respect to the variation of wind speeds. The first mode's damping coefficients increase up to about 1.3% as the wind speeds increase up to 20 m/s. The second mode's damping coefficients fluctuate 0.5~2.5% as the wind speeds change 3~20 m/s. For the fourth and sixth modes, the linear and quadratic functions are well-matched each other. Those modes' damping properties fluctuate 0.5~2.0% as the wind speeds change; however, there are no apparent trends of decrement or increment as the wind speeds change.

3.3 Typhoon-induced variation of dynamic characteristics of the cables

3.3.1 Acceleration and frequency responses of the cables

During the strong wind events of the two consecutive typhoons, the maximum wind speeds and the maximum accelerations of the cables C3 and C5 were monitored by the wireless vibration sensor nodes (Imote2/SHM-A). The magnitudes of the acceleration responses observed during the typhoons' passing were very larger than those recorded in normal wind condition. As shown in Fig. 16, wind speeds and vibration responses are proportionally well matched each other. As shown in the figure, the shortest cable C3 of the side-span had the maximum acceleration response about 0.095 g at the maximum wind speed during the typhoon Bolaven. The cable C5 of the mid-span had the maximum acceleration response about 0.10 g at the maximum wind speed during the typhoon Bolaven.
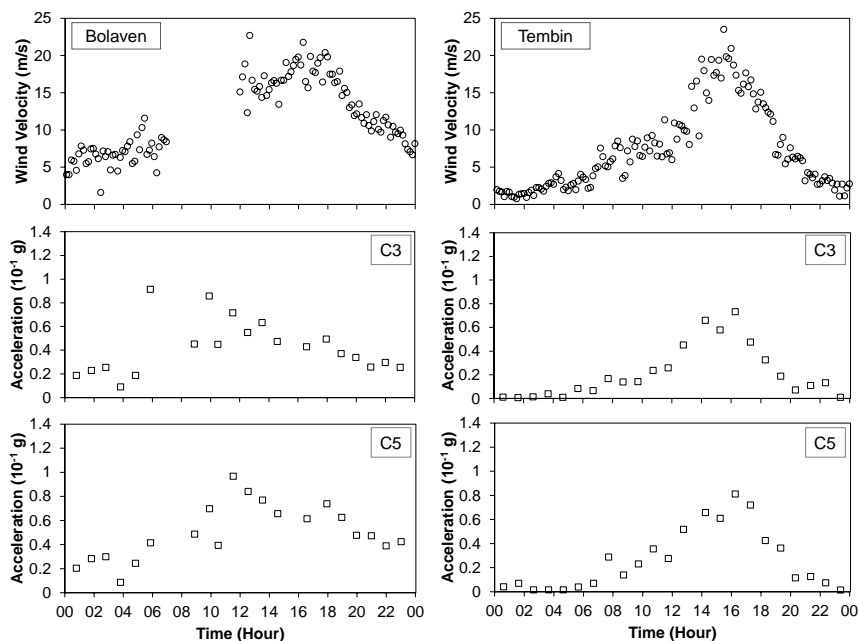

Fig. 16 Wind speeds and maximum acceleration responses of the cable C3 and C5 during two typhoons Bolaven and Tembin

(a) Acceleration and PSD responses at C3

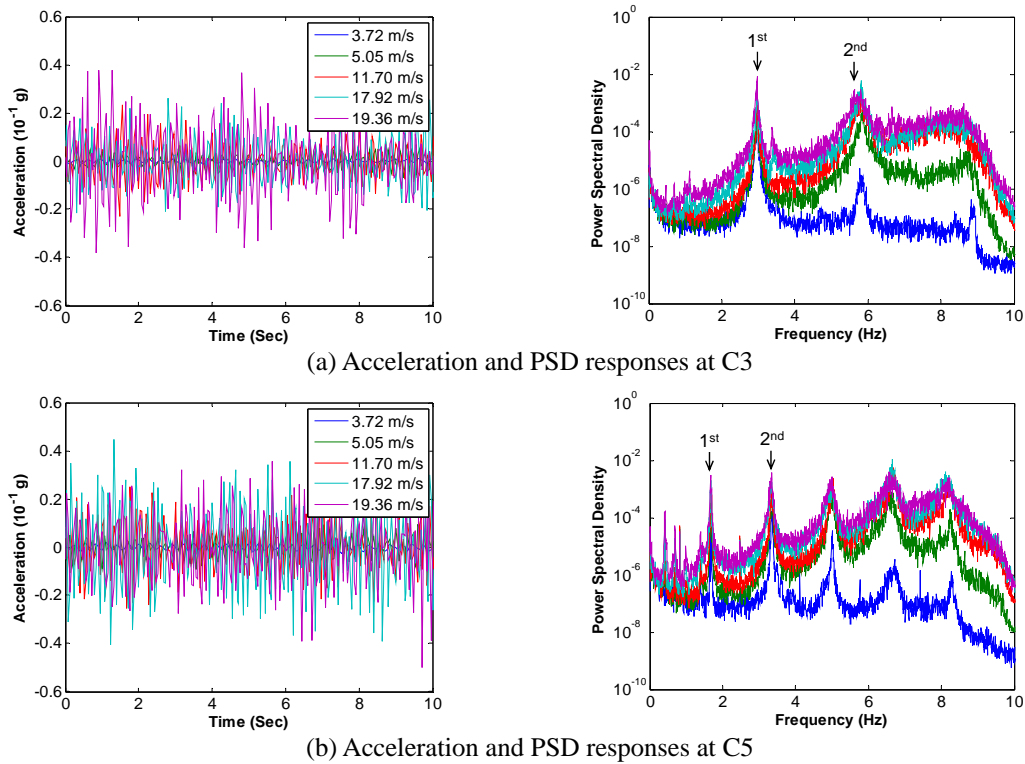(b) Acceleration and PSD responses at C5

Fig. 17 Acceleration and frequency responses of the cable during typhoons

As shown in Fig. 17, acceleration and frequency responses of the cables were recorded for five different wind speeds: 3.72 m/s, 5.05 m/s, 11.70 m/s, 17.92 m/s, and 19.36 m/s. Fig. 17(a) shows wind-induced changes in acceleration and PSD responses measured at the cable C3. Acceleration levels change about 25 times (e.g., 0.0015g – 0.038g) due to the change in wind speeds. The PSD responses of the cable C3 indicate the first three resonance peaks and their changes due to the change in wind speeds. Fig. 17(b) shows wind-induced changes in acceleration and PSD responses measured at the cable C5 for the five wind speeds. Acceleration levels change about 25 times (0.002 g – 0.05 g) due to the change in wind speeds. The PSD responses of the cable C5 indicate the first three resonance peaks and their changes due to the change in wind speeds.

3.3.2 Wind speeds versus modal parameters of cables

Natural frequencies of the cables during the attack of Bolaven and Tembin were extracted from the acceleration signals by using the automated peak-picking algorithm. For the shortest cable C3 and the longest cable C5, the relationships between the wind speeds and the natural frequencies of the first two modes were analyzed, respectively, as shown in Fig. 18 (i.e., the cable C3) and Fig. 19 (i.e., the cable C5). The first and second modes show linear functions with respect to the variation of wind speeds. There seems to be clear trends between the cable frequencies and the wind velocities.
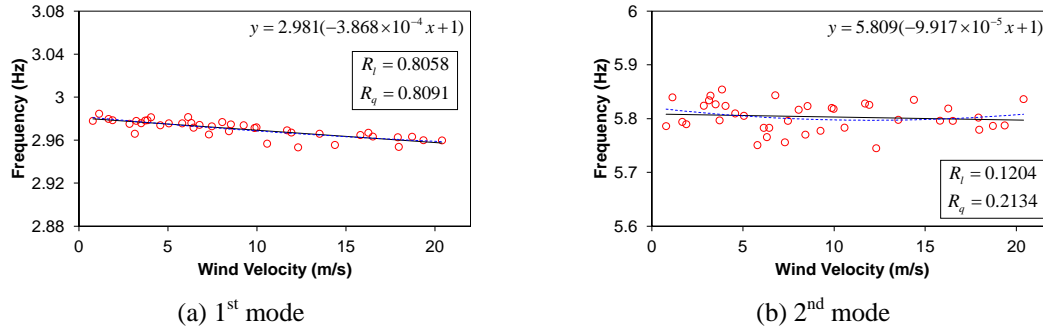
(a) 1st mode (b) 2nd mode

Fig. 18 Relationships between wind velocity and two natural frequencies of the cable C3 during typhoons

Generally, results reveal that the natural frequencies decrease as the wind speeds increase. The first mode's natural frequencies decrease up to about 0.8% (2.98 Hz~2.96 Hz) in the cable C3 and 0.1% (1.679 Hz~1.678 Hz) in the cable C5 as the wind speeds increase up to 20 m/s. The second mode's natural frequencies decrease 0.2% in C3 and 0.04% in C5 as the wind speeds vary 1~20 m/s. The change of natural frequencies is more apparent in the shortest cable C3 than the longest cable C5 in which natural frequencies almost did not change due to the variation of wind speeds.

Modal damping coefficients of the cables during the attack of Bolaven and Tembin were extracted from the acceleration signals by using the SSI algorithm. For the shortest cable C3 and the longest cable C5, the relationships between the wind speeds and the modal damping properties of the first two modes were analyzed, respectively, as shown in Figs. 20 and 21. For the shortest cable C3, the first mode shows linear function but the second mode shows quadratic functions with respect to the variation of wind speeds. There seems to be clear trends between the cable's damping properties and the wind velocities. The results reveal that the damping coefficients increase as the wind speeds increase. The first mode's damping coefficients increase up to about 0.7% as the wind speeds increase up to 20 m/s. The second mode's damping coefficients fluctuate 0.05~2.5% as the wind speeds change 3~20 m/s.

For the longest cable C5, the first mode shows linear function but the second mode shows quadratic functions with respect to the variation of wind speeds. There seems to be clear trends between the cable's damping properties and the wind velocities. The results reveal that the damping coefficients increase as the wind speeds increase. The first mode's damping coefficients fluctuate 0.1~0.8% as the wind speeds increase up to 20 m/s. The second mode's damping coefficients fluctuate 0.05~0.9% as the wind speeds change 3~20 m/s. The change of modal damping properties is not apparent both in the shortest cable C3 than the longest cable C5.

4. Time-frequency analysis by STFT

4.1 STFT analysis of the deck

To identify typhoon-induced variation of dynamic characteristics, time-frequency analyses were performed for the deck vibration signals. The STFT method described in Eq. (4) was utilized to analyze non-stationary random acceleration signals induced by the two typhoons. A rectangular

window with the length of 8196 was used for the STFT and the time resolution was set to one second (e.g., data length of 25). Fig. 22 shows time-frequency STFT analysis of the deck D5 acceleration signals recorded for 10 minutes under wind velocity 4.04 m/s. For the four modes (1st mode, 2nd mode, 4th mode, and 6th mode), natural frequencies are plotted as functions of time.
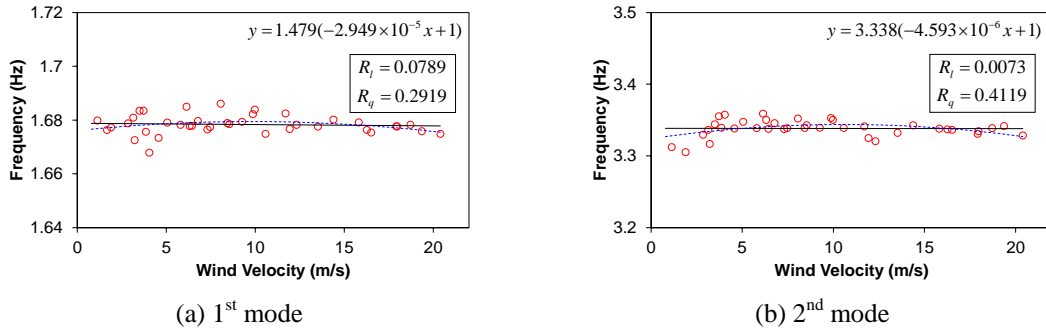
$$y = 1.479(-2.949 \times 10^{-5} x + 1)$$
$$R_l = 0.0789$$
$$R_q = 0.2919$$

$$y = 3.338(-4.593 \times 10^{-6} x + 1)$$
$$R_l = 0.0073$$
$$R_q = 0.4119$$

(a) 1st mode

(b) 2nd mode

Fig. 19 Relationships between wind velocity and two natural frequencies of the cable C5 during typhoons

$$y = 0.107(0.197 x + 1)$$
$$R_l = 0.7230$$
$$R_q = 0.7444$$

$$R_l = 0.3657$$
$$R_q = 0.4510$$
$$y = 0.772(0.0417 x + 1)$$

(a) 1st mode

(b) 2nd mode
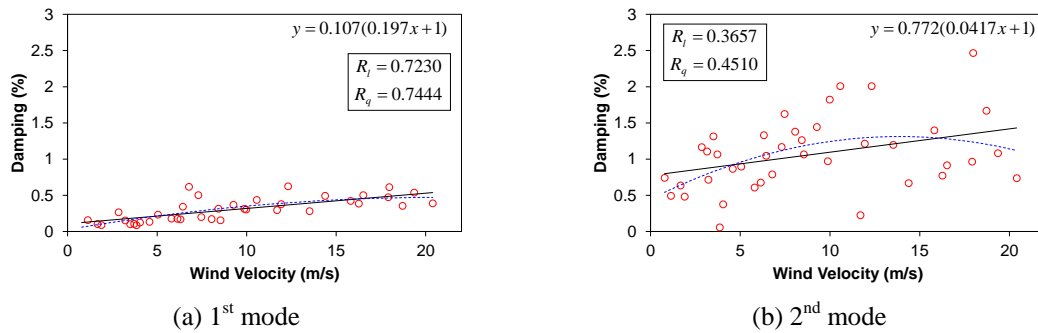
Fig. 20 Relationships between wind velocity and two modal damping coefficients of the cable C3 during typhoons

$$y = 0.379(3.668 \times 10^{-3} x + 1)$$
$$R_l = 0.0544$$
$$R_q = 0.2423$$

$$y = 0.248(0.123 x + 1)$$
$$R_l = 0.7959$$
$$R_q = 0.7974$$

(a) 1st mode

(b) 2nd mode

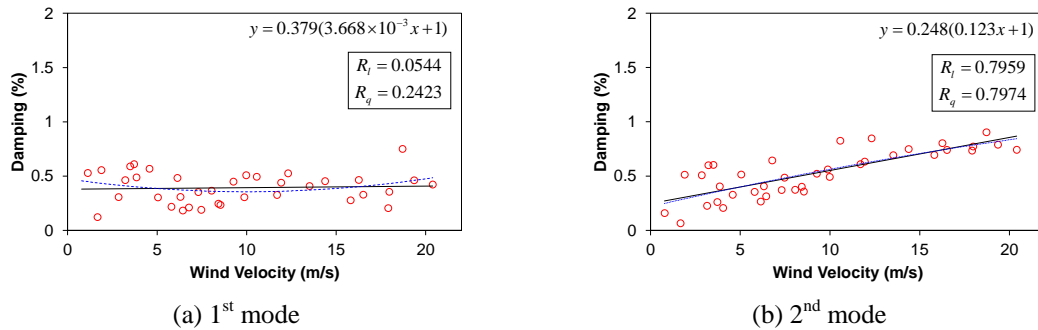Fig. 21 Relationships between wind velocity and two modal damping coefficients of the cable C5 during typhoons

(a) 1st Mode

(b) 2nd Mode
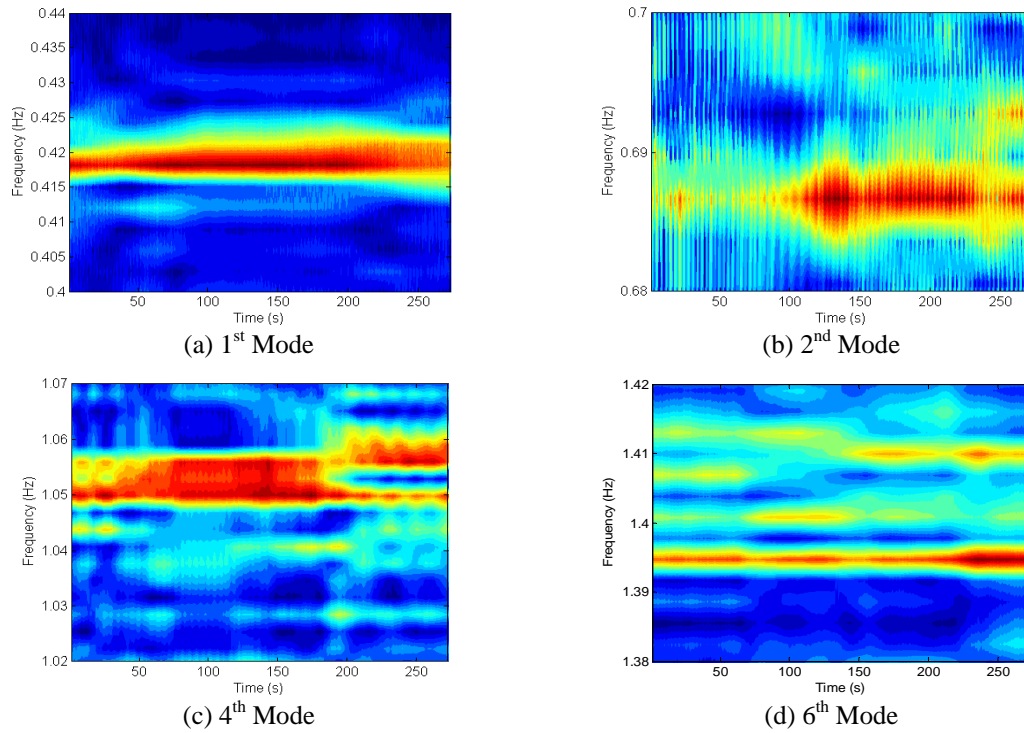
(c) 4th Mode

(d) 6th Mode

Fig. 22 Time-frequency STFT analysis of the deck D5 vibration responses under wind velocity 4.04 m/s

The 4th mode was selected to examine the effect of wind velocity on the natural frequencies. For the 4th mode, the STFT analyses on the deck D5 acceleration signals were performed for three wind speeds (i.e., 5.05 m/s, 11.70 m/s, and 19.36 m/s). As shown in Fig. 23, time-frequency results were analyzed and also compared with those from Welch's and SSI methods described in the previous section. It is observed that natural frequencies decrease as the wind speed increase. It is also observed that the STFT analyses produce natural frequencies fluctuating along with the short period while other two methods (i.e., Welch's and SSI) estimate constant values for the time period. The fluctuating variation in natural frequencies quite increase as the wind speed reaches about 20 m/s.

4.2 STFT analysis of the cables

Time-frequency analyses were performed to identify typhoon-induced variation of dynamic characteristics of the cable. Fig. 24 shows time-frequency STFT analysis of the cables' vibration signals recorded for 10 minutes under wind velocity 4.04 m/s. For the shortest cable C3 and the longest cable C5, natural frequencies of the first mode are plotted as functions of time. The 1st mode was utilized to examine the effect of wind velocity on the cables' natural frequencies. The STFT analyses on the cables' acceleration signals were performed for three wind speeds (i.e., 5.05 m/s, 11.70 m/s, and 19.36 m/s).
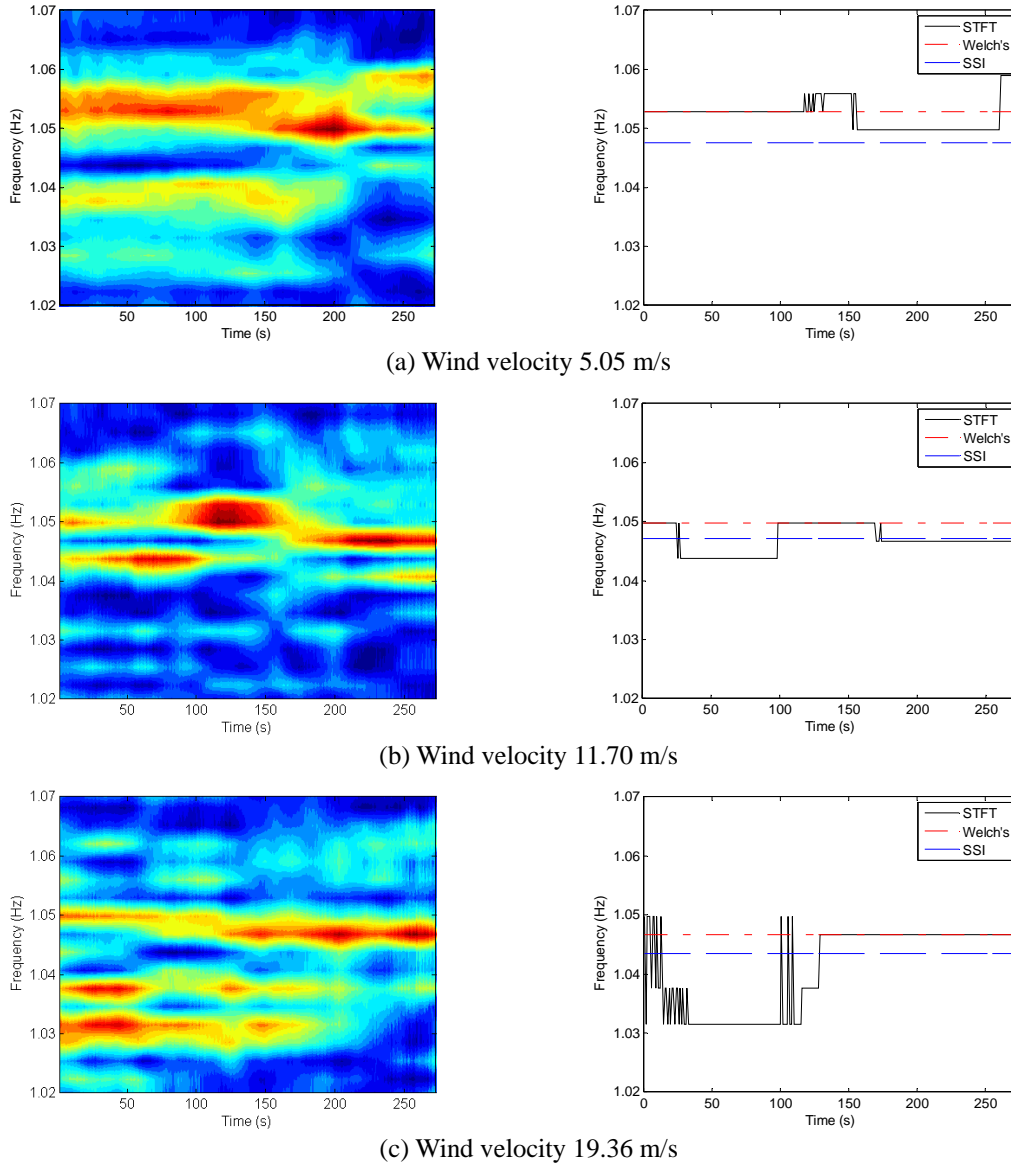
(a) Wind velocity 5.05 m/s

(b) Wind velocity 11.70 m/s

(c) Wind velocity 19.36 m/s

Fig. 23 Mid-span (D5) deck vibration analysis by STFT and frequency variation: 4th Mode

For the cables C3 and C5, time-frequency results were analyzed for each wind-speed case and also compared with those from Welch's and SSI methods described in the previous section, as shown in Figs. 25 and 26. It is observed that natural frequencies decrease as the wind speed increase. It is also observed that the STFT analyses produce natural frequencies fluctuating along with the short period while other two methods (i.e., Welch's and SSI) estimate constant values for the time period. Relative to the longest cable C5, the shortest cable C3 shows quite high variation in natural frequencies as the wind speed reaches about 20 m/s.
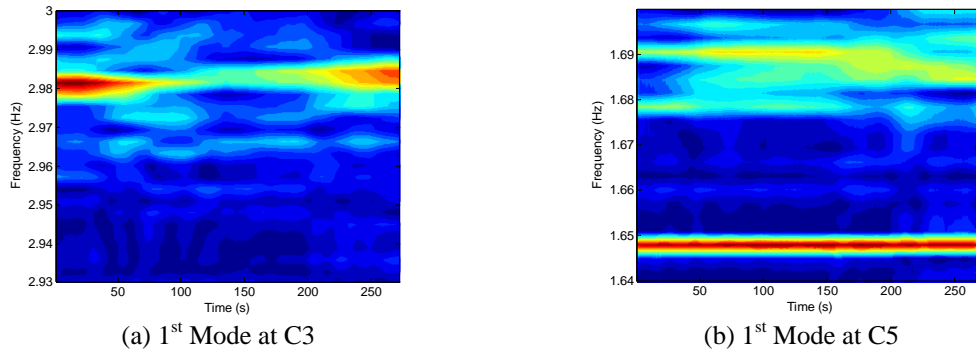
(a) 1st Mode at C3   (b) 1st Mode at C5

Fig. 24 Time-frequency STFT analysis of the cables' vibration responses under wind velocity 4.04 m/s

(a) Wind velocity 5.05 m/s

(b) Wind velocity 11.70 m/s

(c) Wind velocity 19.36 m/s
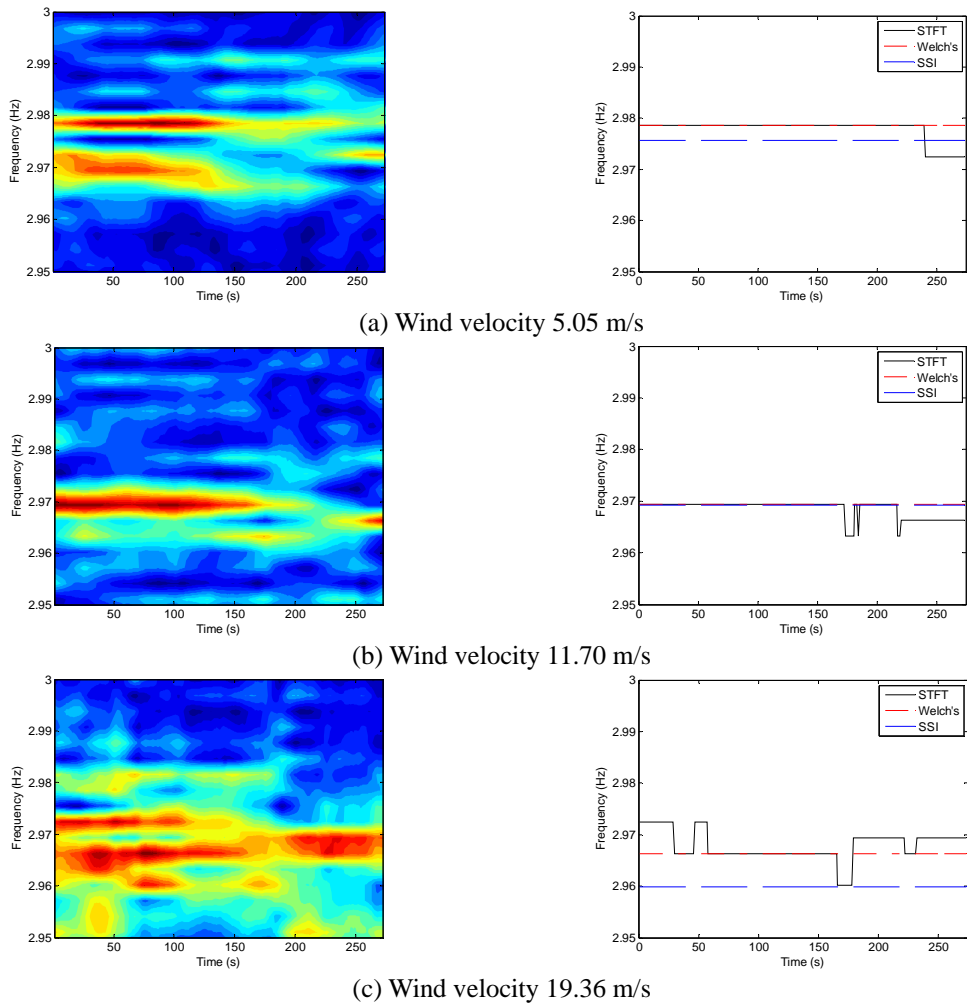
Fig. 25 Short cable (C3) vibration analysis by STFT and frequency variation: 1st Mode

(a) Wind velocity 5.05 m/s

(b) Wind velocity 11.70 m/s
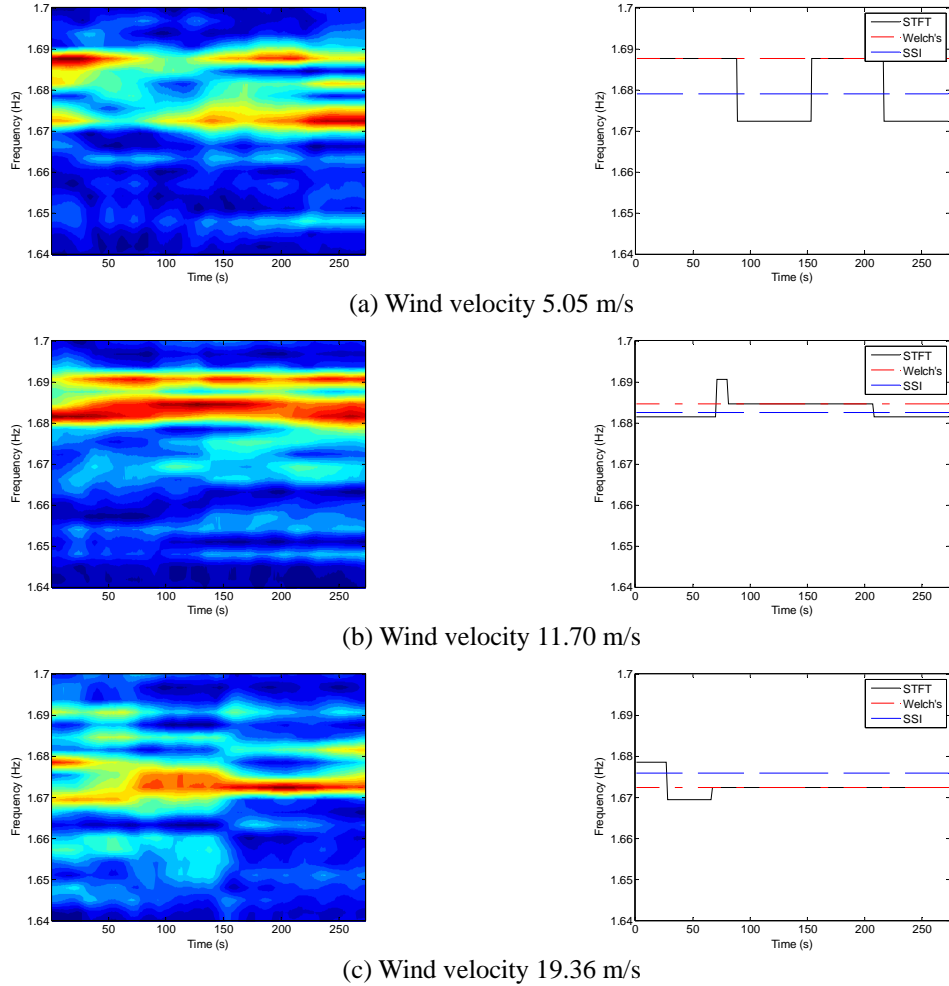

(c) Wind velocity 19.36 m/s

Fig. 26 Long cable (C5) vibration analysis by STFT and frequency variation: 1st Mode

5. Conclusions

In this paper, wireless monitoring of typhoon-induced variation of dynamic characteristics of a cable-stayed bridge was presented. Firstly, cable-stayed bridge with the wireless monitoring system was described. Wireless vibration sensor nodes were utilized to measure accelerations from bridge deck and stay cables. Secondly, dynamic responses of the cable-stayed bridge under the attack of the two typhoons were analyzed by estimating relationships between wind velocity and dynamic characteristics under the two consecutive typhoons, Bolaven and Tembin. Finally, time-varying analyses were performed to investigate non-stationary random properties of the dynamic responses under the typhoons.

Vibration responses were wirelessly monitored from a few survived sensor nodes of the deck (the side-span and the mid-span ones) during the two consecutive typhoons. The relationship between wind velocity and dynamic characteristics of the deck were analyzed as follows: firstly,

acceleration levels change about 17 times as wind speeds varied 3~20 m/s; secondly, natural frequencies decreased up to about 0.8% as the wind speeds increased up to 20 m/s; finally, modal damping coefficients fluctuated 0.5~2.5% as the wind speeds varied 3~20 m/s.

Vibration responses were also monitored from two cables (the shortest and the longest ones). The relationships between wind velocity and dynamic characteristics of the cables were analyzed as follows: firstly, acceleration levels change about 25 times due to the change in wind speeds; secondly, natural frequencies decreased up to about 2.4% in the shortest cable and 0.1% in the longest cable as the wind speeds increased up to 20 m/s; and finally, modal damping coefficients fluctuated 0.05~2.5% in the shortest cable and 0.05~0.9% in the longest cable as the wind speeds changed 3~20 m/s.

The STFT analyses on acceleration signals of the deck and cables produced natural frequencies fluctuating during the short period while other two methods (i.e., Welch's and SSI methods) estimated constant values for the period. The fluctuating variation in natural frequencies quite increased as the wind speed reaches about 20 m/s. Relative to the shortest cable, the longest cable in the middle of the bridge had less variation of natural frequencies.

Acknowledgements

References

Atkan, A.E., Catbas, F.N., Grimmelsman, K.A. and Pervizpour, M. (2003), *Development of a model health monitoring guide for major bridges*, Research Report, Federal Highway Administration Research and Development.

Bendat, J.S. and Piersol, A.G. (1993), *Engineering Applications of Correlation and Spectral Analysis*, Wiley-Interscience, New York, NY, USA.

Bietry, J., Delaunay, D. and Conti, E. (1995), "Comparison of full-scale measurement and computation of wind effects on a cable-stayed bridge", *J. Wind Eng. Ind. Aerod.*, **57**(2-3), 225-235.

Cho, S., Lynch, J.P., Lee, J.J. and Yun, C.B. (2010), "Development of an automated wireless tension force estimation system for cable-stayed bridges", *J. Intell. Mater. Syst. Struct.*, **21**(1), 361-375.

Evans, A.D. and Falvey, R.J. (2012), *Annual Tropical Cyclone Report 2012*, Technical Report, Joint Typhoon Warning Center.

HM Bridge System (2012), http://hmbridge.iptime.org

Ho, D.D., Lee, P.Y., Nguyen, K.D., Hong, D.S., Lee, S.Y., Kim, J.T., Shin, S.W., Yun, C.B. and Shinozuka, M. (2012), "Solar-powered multi-scale sensor node on Imote2 platform for hybrid SHM in cable-stayed bridge", *Smart Struc. Syst.*, **9**(2), 145-164.

Ho, D.D., Nguyen, K.D, Yoon, H.S., and Kim, J.T. (2012), "Multi-scale acceleration-dynamic strain-impedance sensor system for structural health monitoring", *Int. J. Distrib. Sens. N.*, **2012**, 1-17.

Illinois Structural Health Monitoring Project (2010), *Imote2 for Structural Health Monitoring: User's Guide*, University of Illinois at Urbana-Champaign.

Ho, D.D, Ngo, T.M. and Kim, J.T. (2014), "Impedance-based damage monitoring of steel column connection: numerical simulation", *Struct. Monit. Maint.*, **1**(3), 339-356.

Huang, C. and Nagarajaiah, S. (2014), "Experimental study on bridge structural health monitoring using blind source separation method: arch bridge", *Struct. Monit. Maint.*, **1**(1), 69-87.

Jang, S., Jo, H., Cho, S., Mechitov, K., Rice, J.A., Sim, S.H., Jung, H.J., Yun, C.B. and Spencer, B.F. (2010), "Structural health monitoring of a cable-stayed bridges using smart sensor technology: deployment and evaluation", *Smart Struct. Syst.*, **6**(5-6), 439-459.

Jo, H., Rice, J.A., Spencer, B.F., and Nagayama, T. (2010), "Development of a high-sensitivity accelerometer board for structural health monitoring", *Proceedings of the SPIE*, San Diego, March.

Kim, J.T., Park, J.H., Hong, D.S. and Ho, D.D. (2011), "Hybrid acceleration-impedance sensor nodes on Imote2-platform for damage monitoring in steel girder connections", *Smart Struct. Syst.*, **7**(5), 393-416.

Kim, J.T., Huynh, T.C., and Lee, S.Y. (2014), "Wireless structural health monitoring of stay cables under two consecutive typhoons", *Struct. Monit. Maint.*, **1**(1), 47-67.

Ko, J.M. and Ni, Y.Q (2005), "Technology developments in structural health monitoring of large-scale bridges", *Eng. Struct.*, **27**(12), 1715-1725.

Larsen, A. and Larose, G.L. (2015), "Dynamic wind effects on suspension and cable-stayed bridges", *J. Sound Vib.*, **334**, 2-28.

Li, H.N., Yi, T.H., Ren, L., Li, D.S. and Huo, L.S. (2014), "Reviews on innovations and applications in structural health monitoring for infrastructures ", *Struct. Monit. Maint.*, **1**(1), 1-45.

Lynch, J.P. and Loh, K.J. (2006), "A summary review of wireless sensors and sensor networks for structural health monitoring", *Shock Vib. Digest*, **38**(2), 91-128.

Memsic Co. (2010), *Datasheet of ISM400*, http://www.memsic.com

Meyer, J., Bischoff, R., Feltrin, G. and Motavalli, M. (2010), "Wireless sensor networks for long-term structural health monitoring", *Smart Struct. Syst.*, **6**(3), 263-275.

Miller, T.I., Spencer, B.F., Li, J. and Jo, H. (2010), *Solar energy harvesting and software enhancements for autonomous wireless smart sensor networks*, NSEL Report Series, NSEL-022.

Mishra, S.S., Kumar, K. and Krishna, P. (2007), "A study of wind effect on damping and frequency of a long span cable-stayed bridge from rational function approximation of self-excited forces", *Wind Struct.*, **10**(3), 215-232.

Nagayama, T., Sim, S.H., Miyamori, Y. and Spencer, B.F. (2007), "Issues in Structural Health Monitoring Employing Smart Sensors", *Smart Struct. Syst.*, **3**(3), 299-320

Nagayama, T. and Spencer, B.F. (2007), "Structural health monitoring using smart sensors", NSEL Report Series 001, University of Illinois at Urbana-Champaign.

Nguyen, K.D and Kim, J.T. and Park, Y.H. (2013), "Long-Term Vibration Monitoring of Cable-Stayed Bridge Using Wireless Sensor Network", *Int. J. Distrib. Sens. N.*, **2013**, 1-9

Overschee, V.P. and Moor, B. De (1996), *Subspace Identification for Linear System*, Kluwer Academic Publisher, Dordrecht, Netherlands.

Quatieri, T.F. (2001), *Discrete-time Speech Signal Processing: Principles and Practice*, Prentice Hall Press, Upper Saddle River, NJ.

RM Young Co. (2014), http://www.youngusa.com

Rice, J.A. and Spencer, B.F. (2009), *Flexible smart sensor framework for autonomous full-scale structural health monitoring*, NSEL Report Series, NSEL-018.

Spencer, B.F., Ruiz-Sandoval, M.E. and Kurata, N. (2004), "Smart sensing technology: opportunities and challenges", *Struct. Conto. Health Monit.*, **11**(4), 349-368

Yi, J.H. and Yun, C.B. (2004), "Comparative study on modal identification methods using output-only information", *Struct. Eng. Mech.*, **17**(3-4), 445-446

Yi, T.H., Li, H.N. and Gu, M. (2013), "Wavelet based multi-step filtering method for bridge health monitoring using GPS and accelerometer", *Smart Struct. Syst.*, **11**(4), 331-348.

Zhou, H.F., Ni, Y.Q., Ko, J.M. and Wong, K.Y. (2008), "Modeling of wind and temperature effects on modal frequencies and analysis of relative strength of effect", *Wind Struct.*, **11**(1), 35-50